Controlling Spin Current in a Trapped Fermi Gas

X. Du, Y. Zhang, J. Petricka, and J. E. Thomas*

Department of Physics, Duke University, Durham, North Carolina, 27708, USA

(Received 29 April 2009; revised manuscript received 5 June 2009; published 1 July 2009)

We study fundamental features of spin current in a very weakly interacting Fermi gas of ^{6}Li. By creating a spin current and then reversing its flow, we demonstrate control of the spin current. This reversal is predicted by a spin vector evolution equation in energy representation, which shows how the spin and energy of individual atoms become correlated in the nearly undamped regime of the experiments. The theory provides a simple physical description of the spin current and explains both the large amplitude and the slow temporal evolution of the data. Our results have applications in studying and controlling fundamental spin interactions and spin currents in ultracold gases.

DOI: 10.1103/PhysRevLett.103.010401 PACS numbers: 03.75.Ss

Spin dynamics and spin currents have been extensively studied in condensed matter physics [1]. Active manipulation of the electron spin can be used for data processing and storage [2]. For example, a spin current can be used to excite or reverse the magnetization of a nanomagnet [3–5]. In ultracold atomic physics, spin-current-related phenomena have been observed both in a Bose gas [6] and in a Fermi gas [7]. We report on the origin and control of spin current in a weakly interacting Fermi gas.

An optically trapped Fermi gas of ^{6}Li is a rich system in which the strength of interactions between atoms can be controlled by applying a variable bias magnetic field tuned near a Feshbach resonance [8,9]. Close to resonance, the Fermi gas exhibits strong interactions [10], which have been widely studied [11]. This regime offers unprecedented opportunities to test nonperturbative quantum many-body theories. In contrast, little investigation has been done for a weakly interacting Fermi gas, where the s-wave scattering length, a_{12}, for atoms in opposite spin states can be tuned smoothly from small and positive to small and negative. In this regime, spin segregation is observed, where atoms of one spin move outward in the trap, while atoms with the opposite spin move inward. Previous observations of spin segregation [7] have shed new light on the study of this regime.

An overdamped spin-wave theory [12–14] has been used to explain the spin segregation observed in a Bose gas of ^{87}Rb confined in a magnetic trap [6]. In those experiments, the collision rate between the atoms was large compared to the axial trap frequency and sufficient to ensure a thermal momentum distribution. The predictions are in good agreement with the measurements for the Bose gas. In contrast, the corresponding theory of overdamped spin waves for a Fermi gas disagrees with our experiments by 2 orders of magnitude in amplitude, and predicts an oscillation of the density profile, which is not observed [7].

In the ultracold Fermi gas experiments with ^{6}Li, s-wave collisions cannot occur between atoms in the same spin state, due to the Pauli principle. Further, the s-wave scattering length between atoms in opposite spin states is magnetically tuned to be very small. In this case, velocity changing collisions between atoms in different states occur at a rate of only $\sim$0.3 Hz, small compared to both the axial trap frequency and the spin-segregation rate. We explain the observed spin segregation in this regime by a nearly undamped spin wave, in which the spin vector of each atom is correlated with its energy.

To understand the origin of the spin-segregation and corresponding current, consider the evolution of the spin vectors of atoms vibrating almost freely along the axial (long) direction of a cigar-shaped optical trap. Spin-1/2 atoms in states $|\uparrow\rangle$ and $|\downarrow\rangle$ oscillate in the trap with frequencies $\omega_{x\uparrow}$ and $\omega_{x\downarrow}$, respectively. For our trap, $\bar{\omega}_x \equiv (\omega_{x\uparrow} + \omega_{x\downarrow})/2 = 2\pi \times 145$ Hz. As the magnetic moments of the two spin states are not identical, the finite curvature of the bias magnetic field causes a small difference in the axial confining potentials and hence in the oscillation frequencies for the two spin states, $\delta\omega_x \equiv \omega_{x\downarrow} - \omega_{x\uparrow} = -2\pi \times 2.5$ mHz (the corresponding difference in the transverse oscillation frequencies in the optical trap is negligible, due to the tight transverse confinement). The small difference in the axial frequencies correlates the precession rate $\Omega(E)$ of an atomic spin vector in the x-y plane with the energy of the atom. This, along with binary collisions, causes a spin wave.

Figure 1(a) shows that the resonance frequency $\omega_{\rm res}$ for a radio-frequency (rf) transition between states $|n,\uparrow\rangle$ and $|n,\downarrow\rangle$ is shifted by $(n + 1/2)(\omega_{x\downarrow} - \omega_{x\uparrow})$, where n is the harmonic oscillator quantum number for the axial direction, which does not change in the transition. The axial energy E of the atom determines $n + 1/2 = E/\hbar\bar{\omega}_x$. As the velocity changing collision rate for the Fermi gas of ^{6}Li in the experiment is very low compared to the axial trap frequency, collisions do not significantly change the energy of each atom over the time scale of the segregation, and the precession rate can be written as

$$\Omega(E) = -(\delta\omega_x/\bar{\omega}_x)E/\hbar. \quad (1)$$

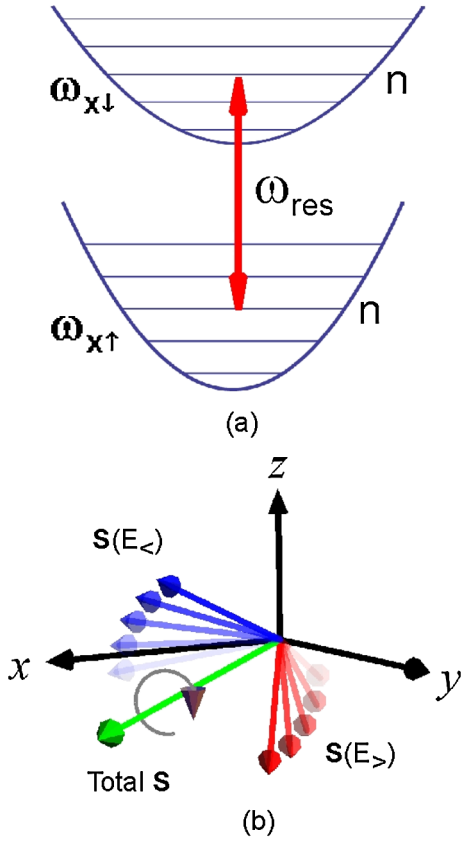

FIG. 1 (color online). Spin-wave formation. (a) For an rf transition between harmonic oscillator-spin states $|n,\uparrow\rangle$ and $|n,\downarrow\rangle$, the resonance frequency $\omega_{\rm res}$ (denoted by the red arrow) decreases with n, due to the difference in the harmonic oscillator frequencies for the two spin states. An rf pulse initially creates x-polarized spins (in the rotating frame). (b) The spin vector for atoms of high energy $E_>$ precesses more than for atoms of low energy $E_<$. Binary collisions then cause the spin vectors to rotate about the total spin vector $\mathbf{S}$, producing a z-polarized spin wave.

As a result of this energy-dependent precession rate, the magnitude of the precession angle of the spin vector in the x-y plane is larger for atoms with high energy than for atoms with low energy.

When two coherently prepared atoms collide, the energy-dependent precession angle then leads to a correlation between the z component of the spin vector and the energy. The collisional interaction results in a rotation of each atom's spin vector about the total spin vector, which is conserved; Fig. 1(b). The sense of the rotation is determined by the sign of the scattering length a_{12}, and the relative angle of the spin vectors. As both atoms have spins in the x-y plane, the rotation of each spin about the total spin in the x-y plane produces spin components out of the x-y plane. For a positive (negative) scattering length, atoms with higher energy $E_>$ will accumulate a negative (positive) z component, while atoms with lower energy $E_<$ will accumulate a positive (negative) z component. This process correlates the z component of the spin with the energy, i.e., $S_z(E)$.

The spin density vector in coordinate space is then determined by the axial harmonic oscillator wave functions $\phi_E(x)$ as $\mathbf{S}(x,t) = \int dE\, \mathbf{S}(E,t)|\phi_E(x)|^2$, where we assume that there is no coherence between different energy states. The energy-dependent spin vector $\mathbf{S}(E,t)$ is determined from the Heisenberg equations $\dot{\hat{\mathbf{S}}}(E,t) = (i/\hbar)\times[\hat{H},\hat{\mathbf{S}}]$, where the components of $\hat{\mathbf{S}}(E,t)$ are written in terms of creation and annihilation operators in energy representation.

In a one-dimensional approximation, the Hamiltonian operator for a Fermi gas in the optical trap is

$$\hat{H} = \hat{H}_0 + \hat{H}_{\rm int}. \tag{2}$$

In a frame rotating at the unshifted hyperfine transition frequency,

$$\hat{H}_0 = \sum_E E(\hat{N}_\uparrow(E) + \hat{N}_\downarrow(E)) + \sum_E \hbar\Omega(E)\hat{S}_z(E), \tag{3}$$

where $\hat{N}_{\uparrow,\downarrow}(E)$ are the number operators for each state and $\hat{S}_z(E) = [\hat{N}_\uparrow(E) - \hat{N}_\downarrow(E)]/2$.

Collisions produce a contact interaction between opposite spin states. Averaging over the transverse coordinates (z, y), the collision operator takes the form

$$\hat{H}_{\rm int} = \frac{4\pi\hbar^2 a_{12}}{m}\frac{1}{2\pi\sigma_\rho^2}\int dx\,\hat{\psi}_\uparrow^\dagger(x)\hat{\psi}_\downarrow^\dagger(x)\hat{\psi}_\downarrow(x)\hat{\psi}_\uparrow(x). \tag{4}$$

Here, m is the atomic mass and σ_ρ is radial $1/e$ width for a fit of a Gaussian distribution of the trapped cloud. Equation (4) can be written in energy representation using $\hat{\psi}_{\uparrow,\downarrow}(x) = \int dE\hat{a}_{\uparrow,\downarrow}(E)\phi_E(x)$.

Using $\mathbf{S}(E,t) = \langle\hat{\mathbf{S}}(E,t)\rangle$, we obtain the evolution equations

$$\frac{\partial\mathbf{S}(E,t)}{\partial t} = \mathbf{\Omega}(E)\times\mathbf{S}(E,t) + \int dE' g(E',E)\mathbf{S}(\mathbf{E}',\mathbf{t})\times\mathbf{S}(\mathbf{E},\mathbf{t}), \tag{5}$$

where

$$g(E',E) = -\frac{4\pi\hbar a_{12}}{m}\frac{1}{\pi\sigma_\rho^2}\left(\frac{m\omega_x^2}{2\pi^4 E_{\rm min}}\right)^{1/2} \times\int_{-(\pi/2)}^{\pi/2}\frac{d\theta}{(\frac{|E-E'|}{E_{\rm min}}+\cos^2\theta)^{1/2}}. \tag{6}$$

Here $E_{\rm min} = \min(E,E')$ and we have assumed a WKB approximation [15] for $\phi_E(x)$ between the classical turning points, since the energies are in the classical regime.

Equation (5) is a primary result of this Letter. The first term describes the energy-dependent spin precession, while the second term describes the rotation of the

spin vector arising from forward scattering in binary collisions. The initial spin vector is $S_x(E, t = 0) = N \exp(-E/K_B T)/(2k_B T)$, where N is the total number of atoms and the factor $1/2$ arises from the definition of the spin vectors. Figure 2 shows that the predictions obtained by numerical integration of Eq. (5) are in good agreement with the data and trap parameters of Ref. [7].

Our description of the spin vector evolution in energy representation can be compared to two recent theories based on a collisionless Boltzmann equation [16,17]. These approaches provide a phase space description in one dimension for a weakly interacting two-component Fermi gas. Their results are in very good agreement with the predictions of Eq. (5), both in amplitude and temporal evolution. We note that Eq. (5) superficially resembles the Landau-Lifshitz-Gilbert (LLG) equation of ferromagnetism [18], which describes the precession and damping of the total magnetization by means of an effective magnetic field that produces a torque. However, Eq. (5) describes the buildup of a correlation between the spin and energy of individual atoms in the completely undamped regime.

The spin-energy correlation description is particularly useful when the energy is nearly conserved, as it provides a very simple physical picture for a weakly interacting spin system. Equation (5) makes it apparent that the spin current can be reversed, causing the spatial distribution to return to the unsegregated state. Two steps are required: A π pulse is applied to reverse the sign of S_z and either S_y or S_x, to rephase the spin vectors; the sign of the scattering length is inverted by sweeping the bias magnetic field through the zero crossing. Then the cloud will start to merge. The quantitative predictions of our numerical simulations are shown in Fig. 3(a). Our experiments confirm this prediction. Immediately after the rf π pulse and inversion of the sign of the scattering length, the difference in the spin-up and spin-down densities at the cloud center is 30% of the average density. As the cloud merges, this difference decreases to zero in ~70 ms, in contrast to the case without current reversal, where spin segregation persists for a few seconds. Then the density difference continues to evolve and returns to 30%.

To perform these experiments, we prepare a spin segregated sample of ^{6}Li Fermi gas at $a_{12} = 8.1 a_0$ [19] (the bias magnetic field $B = 529.8$ G is calibrated by rf spectroscopy). A sample of ^{6}Li atoms in a 50–50 mixture of the two lowest hyperfine states is loaded into a CO_2 laser trap with a bias magnetic field of 840 G, where the two states are strongly interacting. Evaporative cooling is performed to lower the temperature of the sample [10]. The magnetic field is then increased in 0.8 sec to a weakly interacting regime at 1200 G where an on-resonance optical pulse of 40 μs is applied to remove atoms of one state, while

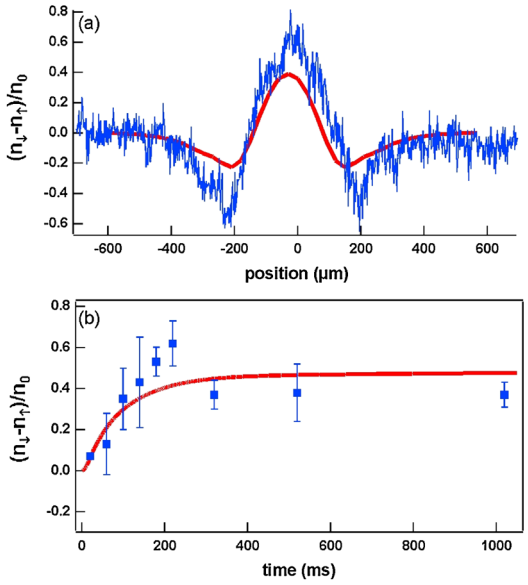

FIG. 2 (color online). (a) Difference between the spin-down and spin-up densities $n_\downarrow - n_\uparrow$ at 220 ms in units of $n_0 = (n_{\downarrow 0} + n_{\uparrow 0})/2$. Here n_{i0} is the initial spin density for each state at the trap center before spin segregation occurs. Data (blue line); theory (red curve). The data are taken for $a_{12} = -4.5 a_0$; (b) $n_\downarrow - n_\uparrow$ at the trap center versus time for $a_{12} = -4.5 a_0$. Data (blue dots); theory (red curve).

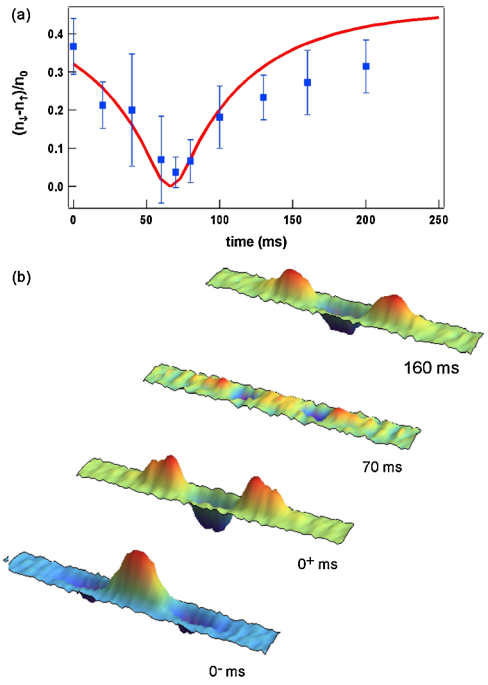

FIG. 3 (color online). Reversal of the spin current in an ultracold Fermi gas. (a) Difference in the spin densities $n_\downarrow - n_\uparrow$ at the trap center versus time, showing return to 0 at $t \simeq 70$ ms, after an rf π pulse is applied and the sign of scattering length is inverted at $t \simeq 0$. Prediction (red line); data (blue dots). (b) Images of the spin waves corresponding to the time in (a). Each image is the z component of the spin density as a function of position x along the axial direction of the trap. 0^- ms corresponds to time just before the rf π pulse and 0^+ ms corresponds to time just after the rf π pulse and reversal of the scattering length.

leaving atoms in the other state. With a single state present, the magnetic field is lowered in 0.8 sec to 529.8 G. Then a 40 ms rf pulse (center frequency 75.613 MHz and sweep range 35 kHz) is applied on the $|\uparrow\rangle - |\downarrow\rangle$ transition to create a 50–50 coherent superposition of the two spin states. Note that, as the frequency passes through resonance, coherence is created on a time scale of a few milliseconds, short compared to the time for the total sweep and for spin segregation to occur. At the final optical trap depth, the measured trap oscillation frequency in the transverse directions is $\omega_\perp = 2\pi \times 3900$ Hz, while the axial frequency is $\omega_x = 2\pi \times 120$ Hz. The total number of atoms is $N \simeq 4.0 \times 10^5$. The corresponding Fermi temperature is $T_F \simeq 6$ μK. The sample temperature is $T \simeq 33$ μK. The peak atomic density at T is $6 \times 10^{11}/\mathrm{cm}^3$. The axial and radial $1/e$ widths for a fit of a Gaussian distribution to the initial density profile of the sample are $\simeq 400$ and $\simeq 12$ μm, respectively.

At 40 ms after the first rf pulse, when difference in the spin-up and spin-down densities is 30% of the average density, we change the bias magnetic field from 529.8 G ($a_{12} = 8.1a_0$) to 525.2 G ($a_{12} = -8.1a_0$) in 5 ms. Then we apply an rf π pulse (duration 40 ms, center frequency 75.596 MHz and sweep range 4 kHz), which flips the spins, as shown in the 0^- and 0^+ images of Fig. 3(b). Finally, we take absorption images of atoms in both states (in separate experimental cycles) at various times after the rf π pulse, Fig. 3 [20]. The entire time sequence is done in random order and repeated 6 times. The error bars are statistical and arise from run-to-run variations in the atom number, magnetic field and excitation frequency.

As a further test of this idea, we applied either the scattering length sign change or the rf π pulse, but not both, and looked for merging followed by segregation. We found no reversal of spin segregation. This verifies that both operations are required to observe the reversal of spin segregation, as predicted.

In an additional experiment, we increased the length of the initial spin-segregation time, to determine the longest time scale τ over which the spin segregation is reversible. We expect that τ must be significantly smaller than the velocity changing collision time (~ 3 sec) for reversal to occur and find $\tau = 200$ ms.

In conclusion, we have developed a physically intuitive energy-space description of the spin dynamics of a Fermi gas in the nearly undamped regime. This picture suggests that broad manipulation of the spin dynamics and creation and study of nonequilibrium systems in arbitrary spin mixtures is possible, by using general rf pulse sequences and by temporally and spatially varying both the scattering lengths and the energies of the spin components. As an example, we have predicted and experimentally verified rephasing of the spin vectors and reversal of the spin current, i.e., a "spin-current echo," by simultaneously applying a π pulse and reversing the sign of the scattering length.

This research is supported by the Physics Divisions of the Army Research Office and the National Science Foundation, and the Chemical Sciences, Geosciences and Biosciences Division of the Office of Basic Energy Sciences, Office of Science, U.S. Department of Energy. We thank Paul Julienne for providing the magnetic field dependence of the scattering length near the zero crossing and Le Luo and Bason Clancy for help during the initial stages of these experiments. Finally, we are indebted to Franck Laloë for stimulating discussion and for pointing out an error in Eq. (6) of the original manuscript.

*jet@phy.duke.edu

[1] I. Žutić, J. Fabian, and S. D. Sarma, Rev. Mod. Phys. **76**, 323 (2004).
[2] S. Das Sarma, Am. Sci. **89**, 516 (2001).
[3] R. Duine, Physics **1**, 27 (2008).
[4] J. Slonczewski, J. Magn. Magn. Mater. **159**, L1 (1996).
[5] L. Berger, Phys. Rev. B **54**, 9353 (1996).
[6] H. J. Lewandowski, D. M. Harber, D. L. Whitaker, and E. A. Cornell, Phys. Rev. Lett. **88**, 070403 (2002).
[7] X. Du, L. Luo, B. Clancy, and J. E. Thomas, Phys. Rev. Lett. **101**, 150401 (2008).
[8] E. Tiesinga, A. J. Moerdijk, B. J. Verhaar, and H. T. C. Stoof, Phys. Rev. A **46**, R1167 (1992).
[9] E. Tiesinga, B. J. Verhaar, and H. T. C. Stoof, Phys. Rev. A **47**, 4114 (1993).
[10] K. M. O'Hara, S. L. Hemmer, M. E. Gehm, S. R. Granade, and J. E. Thomas, Science **298**, 2179 (2002).
[11] S. Giorgini, L. P. Pitaevskii, and S. Stringari, Rev. Mod. Phys. **80**, 1215 (2008).
[12] M. Ö. Oktel and L. S. Levitov, Phys. Rev. Lett. **88**, 230403 (2002).
[13] J. N. Fuchs, D. M. Gangardt, and F. Laloë, Phys. Rev. Lett. **88**, 230404 (2002).
[14] J. E. Williams, T. Nikuni, and C. W. Clark, Phys. Rev. Lett. **88**, 230405 (2002).
[15] J. J. Sakurai, *Modern Quantum Mechanics* (Addison-Wesley, Reading, MA, 1993).
[16] F. Piéchon, J. N. Fuchs, and F. Laloë, Phys. Rev. Lett. **102**, 215301 (2009).
[17] S. S. Natu and E. J. Mueller, Phys. Rev. A **79**, 051601 (2009).
[18] T. L. Gilbert, IEEE Trans. Magn. **40**, 3443 (2004).
[19] M. Bartenstein *et al.*, Phys. Rev. Lett. **94**, 103201 (2005).
[20] The numerical simulation shows the merging time, i.e., time for segregation to disappear, is equal to the waiting time for segregation before the π rf pulse. The waiting time is estimated as 65 ms, including 40 ms (time period between end of the first rf pulse and start of magnetic field switch), 20 ms (half of the first rf pulse duration), and 5 ms (magnetic field switch time).